
FAST PDE-CONSTRAINED OPTIMIZATION VIA SELF-SUPERVISED OPERATOR LEARNING

A PREPRINT

Sifan Wang

Graduate Group in Applied Mathematics
and Computational Science
University of Pennsylvania
Philadelphia, PA 19104
sifanw@sas.upenn.edu

Mohamed Aziz Bhouri

Department of Mechanical Engineering
and Applied Mechanics
University of Pennsylvania
Philadelphia, PA 19104
bhouri@seas.upenn.edu

Paris Perdikaris

Department of Mechanical Engineering
and Applied Mechanics
University of Pennsylvania
Philadelphia, PA 19104
pgp@seas.upenn.edu

October 27, 2021

ABSTRACT

Design and optimal control problems are among the fundamental, ubiquitous tasks we face in science and engineering. In both cases, we aim to represent and optimize an unknown (black-box) function that associates a performance/outcome to a set of controllable variables through an experiment. In cases where the experimental dynamics can be described by partial differential equations (PDEs), such problems can be mathematically translated into PDE-constrained optimization tasks, which quickly become intractable as the number of control variables and the cost of experiments increases. In this work we leverage physics-informed deep operator networks (DeepONets) – a self-supervised framework for learning the solution operator of parametric PDEs – to build fast and differentiable surrogates for rapidly solving PDE-constrained optimization problems, even in the absence of any paired input-output training data. The effectiveness of the proposed framework will be demonstrated across different applications involving continuous functions as control or design variables, including time-dependent optimal control of heat transfer, and drag minimization of obstacles in Stokes flow. In all cases, we observe that DeepONets can minimize high-dimensional cost functionals in a matter of seconds, yielding a significant speed up compared to traditional adjoint PDE solvers that are typically costly and limited to relatively low-dimensional control/design parametrizations.

Keywords Deep learning · Design optimization · Optimal control · Computational physics

1 Introduction

Motivation: A ubiquitous task across many disciplines in science and engineering is to optimize the performance of a system governed by physical laws that are mathematically expressed as systems of partial differential equations (PDEs). Many of such tasks can be formally formulated as PDE-constrained optimization problems which naturally arise in various settings such as shape optimization [1, 2], optimal control [3], image processing [4], aerodynamics [5, 6], crystal growth [7], drug delivery [8], heat transfer phenomena [9, 10] and finance [11]. Despite their prominence, PDE-constrained optimization problems are notoriously hard to solve, especially in cases where the cost of simulating the PDE system is high and the number of design/control parameters is large. The latter can quickly lead to intractable

complexity, often referred to as the *curse of dimensionality*, as a naive exploration of the decision space via grid search requires a number of experiments that grow exponentially with the dimension of the design/control parameters. Even more severe is the setting where those design/control parameters are not finite-dimensional vectors, but continuous functions with infinitely many degrees of freedom.

Related work: A large volume of literature has focused on designing effective solutions for tackling PDE-constrained optimization problems, primarily by developing fast emulators and surrogate models that can bypass the cost of expensive experiments [12, 13, 14], as well as formulating effective strategies for exploring the input parameter space, for example using gradient-based methods [15], adjoint solvers [16, 17], or Bayesian optimization [18, 19]. Fast emulators are typically built by reduced-order modeling techniques [20, 21] formulated on the premise that solutions of parametric PDEs live on a low-dimensional manifold. Given a (typically large) number of high-fidelity realizations of the original system that sufficiently span the parameter space, one can discover the low-dimensional manifold using techniques such as principal components analysis [22, 23, 24], diffusion maps [25], or auto-encoders [26, 27, 28]. If successful, then one can simulate the system’s performance given a new design/control input using far less degrees of freedom compared to the full-order experiment, yielding often dramatic computational speed-ups, but often at the price of reduced fidelity [29, 30]. While reduced-order models are currently one of the main workhorses for PDE-constrained optimization [20, 31], their construction can be computationally expensive as it requires accumulating a large number of system responses to input excitations. Furthermore, they usually lack robustness with respect to parameter changes and therefore must often be rebuilt for each parameter variation [30]. As such, their effectiveness can quickly deteriorate as the number of input design/control variables increases.

More recently, deep learning approaches have been used to tackle PDE-constrained tasks across diverse applications, including electromagnetism [32], nanophotonics [33], material science [34], structural mechanics [35], and optimal control [36]. However, many of these approaches still rely on traditional numerical solvers and require an excessive amount of training data that can be costly to obtain, while their predictions are typically not consistent with the underlying PDE that generated the training data [37]. The latter can be addressed by adopting frameworks such as physics-informed neural networks (PINNs) [38, 39, 40]. However, PINNs are known to be notoriously hard to train [41, 42, 43], and can incur a large computational cost during the online phase of a PDE-constrained optimization task as they may need to be re-trained in order to accurately generalize across different design/control inputs.

Contributions of this work: In this work we propose to leverage physics-informed deep operator networks (DeepONets) [37, 44, 45]; a recently developed deep learning framework for learning the solution operator of parametric PDEs in a self-supervised manner. This enables the construction of effective emulators for querying the solution of PDEs at an arbitrary spatio-temporal resolution, given continuous (i.e. infinite-dimensional) design/control inputs, and without the requirement of generating large training data-sets via repeatedly evaluating costly conventional simulators. As we shall see, a trained physics-informed DeepONet model can be used as a fast and differentiable surrogate for tackling high-dimensional PDE-constrained optimization problems via gradient-based optimization in near real-time. The effectiveness of the proposed framework will be demonstrated through different case studies in optimal control and shape optimization, demonstrating a significant speed up compared to traditional adjoint finite element solvers.

Structure of this paper: In section 2, we formulate general PDE-constrained optimization tasks and present a brief overview of physics-informed DeepONets. Next, we describe how a trained physics-informed DeepONet model can be leveraged as a fast and differentiable surrogate for rapidly solving PDE-constrained optimization problems. In section 3, we perform a series numerical studies to demonstrate the effectiveness of the proposed framework. Finally, section 4 concludes with a discussion of our main findings, potential pitfalls, and shortcomings, as well as future research directions emerging from this study. All code and data accompanying this manuscript will be made available at <https://github.com/PredictiveIntelligenceLab/PDE-constrained-optimization-PI-DeepONet>.

2 Methods

2.1 PDE-constrained optimization

We begin with defining PDE-constrained optimization problems in an abstract form. Let U, S, V be Banach spaces, and consider the following general PDE-constrained optimization problem

$$\min \mathcal{J}(\mathbf{u}, \mathbf{s}) \tag{2.1}$$

$$\text{s.t. } \mathcal{E}(\mathbf{u}, \mathbf{s}) = 0 \tag{2.2}$$

$$\mathbf{u} \in U_{ad}, \mathbf{s} \in S_{ad}, \tag{2.3}$$

where $\mathcal{J} : U \times S \rightarrow \mathbb{R}$ denotes a cost function to be minimized, and $\mathcal{E} : U \times S \rightarrow V$ represents a system of PDEs subject to appropriate initial and boundary conditions. Moreover, the latent state \mathbf{s} that satisfies the PDE system is

assumed to belong to an admissible space of functions $S_{ad} \subset S$, while the associated control/input functions \mathbf{u} belong to an admissible function space $U_{ad} \subset U$. Here we assume that for every $\mathbf{s} \in S_{ad}$, there exists a unique $\mathbf{u} = \mathbf{u}(\mathbf{s})$ such that $\mathcal{E}(\mathbf{u}, \mathbf{s}) = 0$. Consequently, we can define the PDE solution operator $G : U \rightarrow S$ that maps input control functions \mathbf{u} to their associated PDE solutions \mathbf{s} as $G(\mathbf{u}) = \mathbf{s}$.

2.2 Physics-informed DeepONets

Deep operator networks (DeepONets) [46] provide a specialized deep learning framework that aims to learn abstract nonlinear operators between infinite-dimensional function spaces. The architecture is inspired and validated by the rigorous universal approximation theorem for operators [47, 46]. In follow up work, Wang *et al.* [37] developed physics-informed DeepONets, introducing a simple and effective regularization mechanism for biasing the outputs of DeepONet models towards ensuring physical consistency. Here we give a brief overview of physics-informed DeepONets, with a special focus on learning the solution operator of parametric PDEs. The terminology "parametric PDEs" refers to the fact that some parameters of a given PDE system are allowed to vary over a certain range. These input parameters may include, but are not limited to, the shape of the physical domain, the initial or boundary conditions, constant or variable coefficients (e.g. diffusion or reaction rates), source terms, etc. To describe such problems in their full generality, let $(\mathcal{U}, \mathcal{V}, \mathcal{S})$ be a triplet of Banach spaces, and $\mathcal{N} : \mathcal{U} \times \mathcal{S} \rightarrow \mathcal{V}$ be a linear or nonlinear differential operator. We consider general parametric PDEs taking the form

$$\mathcal{N}(\mathbf{u}, \mathbf{s})(\mathbf{x}) = 0, \quad (2.4)$$

subject to boundary conditions

$$\mathcal{B}(\mathbf{u}, \mathbf{s})(\mathbf{x}) = 0, \quad (2.5)$$

where $\mathbf{u} \in \mathcal{U}$ denotes the parameters (i.e. input functions), and $\mathbf{s} \in \mathcal{S}$ denotes the unknown latent quantity of interest that is governed by the PDE system of equation 2.4. Moreover, $\mathcal{N}[\cdot]$ is a differential operator, and $\mathcal{B}[\cdot]$ denotes a boundary conditions operator that enforces any Dirichlet, Neumann, Robin, or periodic boundary conditions. For time-dependent problems, we consider time t as a special component of \mathbf{x} , and Ω is extended to contain the temporal domain. In that case, initial conditions can be simply treated as a special type of boundary condition defined in the joint spatio-temporal domain.

Having assumed that, for any $\mathbf{u} \in \mathcal{U}$, there exists an unique solution $\mathbf{s} = \mathbf{s}(\mathbf{u}) \in \mathcal{S}$ to 2.4 (subject to appropriate initial and boundary conditions), then we can define the solution operator $G : \mathcal{U} \rightarrow \mathcal{S}$ as

$$G(\mathbf{u}) = \mathbf{s}(\mathbf{u}). \quad (2.6)$$

Following the original formulation of Lu *et al.* [46], the solution map G can be represented by an unstacked DeepONet G_θ , where θ denotes all trainable parameters (i.e. weights and biases) of the DeepONet network. As shown in Figure 1, the DeepONet architecture is composed of two separate neural networks referred to as the "branch" and "trunk" networks, respectively. The branch network takes \mathbf{u} as inputs and returns a features embedding $[b_1, b_2, \dots, b_q]^T \in \mathbb{R}^q$ as output, where $\mathbf{u} = [\mathbf{u}(\mathbf{x}_1), \mathbf{u}(\mathbf{x}_2), \dots, \mathbf{u}(\mathbf{x}_m)]$ represents a function $\mathbf{u} \in \mathcal{U}$ evaluated at a collection of fixed locations $\{\mathbf{x}_i\}_{i=1}^m$. The trunk network takes the continuous coordinates \mathbf{y} as inputs, and constructs a features embedding $[t_1, t_2, \dots, t_q]^T \in \mathbb{R}^q$. The final output is obtained by performing the dot product of the outputs of the branch and trunk networks. Specifically, a DeepONet G_θ prediction of a function \mathbf{u} evaluated at \mathbf{y} can be expressed by

$$G_\theta(\mathbf{u})(\mathbf{y}) = \sum_{k=1}^q \underbrace{b_k(\mathbf{u}(\mathbf{x}_1), \mathbf{u}(\mathbf{x}_2), \dots, \mathbf{u}(\mathbf{x}_m))}_{\text{branch}} \underbrace{t_k(\mathbf{y})}_{\text{trunk}}. \quad (2.7)$$

Then, a physics-informed DeepONet model can be trained by minimizing the following composite loss function

$$\mathcal{L}(\theta) = \mathcal{L}_{\text{BC}}(\theta) + \mathcal{L}_{\text{PDE}}(\theta), \quad (2.8)$$

where

$$\mathcal{L}_{\text{BC}}(\theta) = \frac{1}{NP} \sum_{i=1}^N \sum_{j=1}^P \left| \mathcal{B}(\mathbf{u}^{(i)}, G_\theta(\mathbf{u}^{(i)}))(\mathbf{y}_{b,j}^{(i)}) \right|^2 \quad (2.9)$$

$$\mathcal{L}_{\text{PDE}}(\theta) = \frac{1}{NQ} \sum_{i=1}^N \sum_{j=1}^Q \left| \mathcal{N}(\mathbf{u}^{(i)}, G_\theta(\mathbf{u}^{(i)}))(\mathbf{y}_{r,j}^{(i)}) \right|^2. \quad (2.10)$$

Here, $\{\mathbf{u}^{(i)}\}_{i=1}^N$ denotes N separate input functions sampled from \mathcal{U} . For each $\mathbf{u}^{(i)}$, $\{\mathbf{y}_{b,j}^{(i)}\}_{j=1}^P$ are P locations that are determined by the boundary conditions. Besides, $\{\mathbf{y}_{r,j}^{(i)}\}_{j=1}^Q$ is a set of collocation points that can be randomly sampled

in the domain of $G(\mathbf{u}^{(i)})$. As a consequence, $\mathcal{L}_{\text{BC}}(\boldsymbol{\theta})$ fits the initial/boundary conditions, while $\mathcal{L}_{\text{PDE}}(\boldsymbol{\theta})$ enforces the underlying PDE constraints. It is worth emphasizing that the formulation of the physics-informed DeepONets does not require any paired input-output observations for training the model, except for a set of given boundary conditions [37]. We also remark that the DeepONet architecture yields a continuous representation of the output functions that can be differentiated with respect to their input coordinates, thus allowing us to directly compute any given differential constraints via automatic differentiation [48, 49].

2.3 PDE-constrained optimization with physics-informed DeepONets

In this section, we describe our proposed method for solving general PDE-constrained optimization problems (see equations 2.1 - 2.3) using physics-informed DeepONets. As summarized in Algorithm 1, the proposed framework consists of two main steps.

Step 1: In the first step, we represent the PDE solution operator $G : U \rightarrow S$ by a physics-informed DeepONet $G_{\boldsymbol{\theta}}$, which is trained by minimizing the composite loss function in equation 2.8. For every input control function $\mathbf{u} \in U_{ad}$, a trained physics-informed DeepONet can rapidly return the corresponding PDE solution $s(\mathbf{u})$ via a simple model evaluation. Moreover, the DeepONet model predictions are differentiable with respect to the input control functions, allowing us to employ gradient-based optimization to expediently minimize the cost functional \mathcal{J} in equation 2.1.

Step 2: In the second step, we construct a parametrization of the input control functions u_{α} (e.g. a deep neural network, or otherwise) with tunable parameters α , and minimize the cost function 2.1 using gradient descent to identify a locally optimal solution. An illustration of the proposed workflow is presented in Figure 1.

Algorithm 1: PDE-constrained optimization using physics-informed DeepONets.

Step 1: Train a physics-informed DeepONet to learn the PDE solution operator $G : U \rightarrow S$.

- (a) Represent the PDE solution operator by a DeepONet $G_{\boldsymbol{\theta}}$ with parameters $\boldsymbol{\theta}$.
- (b) Prepare the training data for the PDE constraints and boundary conditions according to the system of governing equations $\mathcal{E}(\mathbf{u}, s)$.
- (c) Formulate a physics-informed loss function $\mathcal{L}(\boldsymbol{\theta})$ by considering both the PDE and the boundary condition residuals.
- (d) Train the physics-informed DeepONet to identify a set of optimal parameters $\boldsymbol{\theta}^*$ by minimizing the loss function $\mathcal{L}(\boldsymbol{\theta})$ via a stochastic gradient descent method.

Step 2: Train a neural network to minimize the cost function \mathcal{J} .

- (a) Parametrize the input control functions \mathbf{u}_{α} , where α is a set of tunable parameters that need to be optimized (e.g. the weights and biases of a deep neural network).
- (b) Formulate a loss function $\mathcal{J}(\alpha)$ using the trained physics-informed DeepONet $G_{\boldsymbol{\theta}^*}$ according to the definition of the cost functional in equation 2.1.
- (c) Minimizing the cost functional $\mathcal{J}(\alpha)$ via a gradient descent method to identify the optimal control parameters α^* .

*All gradients (i.e. $\partial\mathcal{L}/\partial\boldsymbol{\theta}$, $\partial\mathcal{J}/\partial\alpha$ and $\partial s/\partial\mathbf{x}$) are computed using automatic differentiation).

3 Results

In the following, we demonstrate the effectiveness of physics-informed DeepONets across a series of numerical studies involving various types of PDE-constrained optimization problems, including optimal control and shape optimization. The hyper-parameter settings, performance metrics, and validation details are discussed in Appendix B, D, and F, respectively. It is worth emphasizing that, in all cases, the proposed deep learning models are trained without any paired input-output data, assuming only knowledge of the underlying governing PDE system and its corresponding initial or boundary conditions. All code and data accompanying this manuscript will be made publicly available at <https://github.com/PredictiveIntelligenceLab/PDE-constrained-optimization-PI-DeepONet>.

3.1 Optimal control of a 1D Poisson equation

We start with a pedagogical example involving optimal control of a 1D Poisson equation. Physically, this problem can be interpreted as finding the optimal heating/cooling of a cooktop to achieve the desired temperature profile.

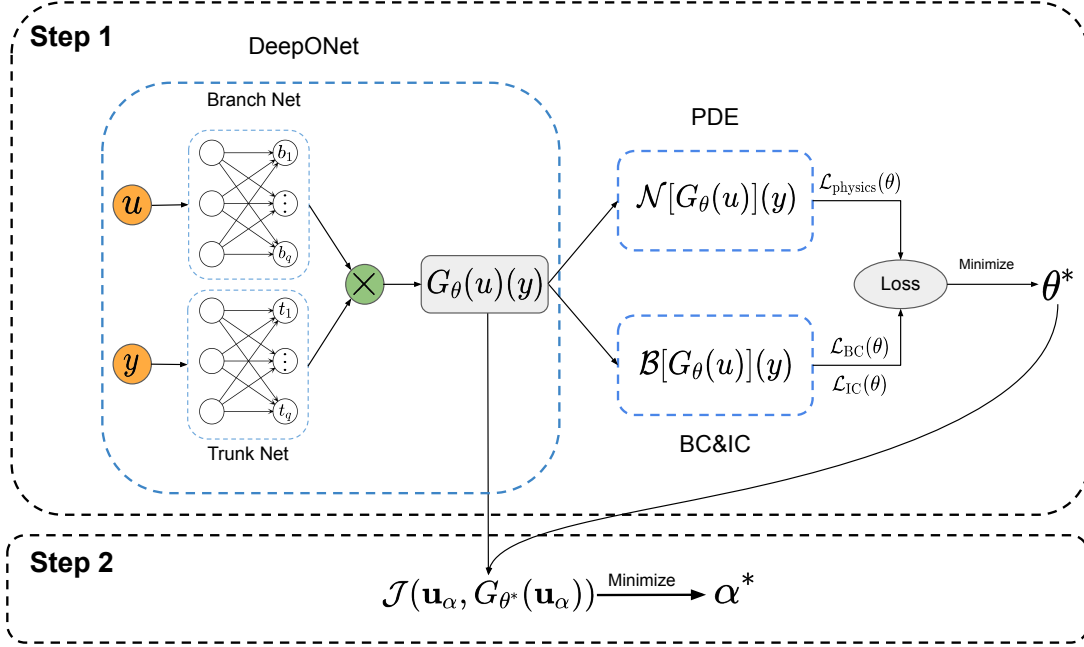


Figure 1: *PDE-constrained optimization workflow*: In Step 1, a physics-informed DeepONet G_θ is trained to learn the solution operator for the given parametric PDE system 2.2. In Step 2, a neural network u_α is employed to represent the control function and then trained by minimizing the cost function \mathcal{J} defined in 2.1 where the trained physics-informed DeepONet is used as a surrogate forward PDE solver. It is worth noting that the algorithm does not require any solution measurements except for a set of boundary and initial conditions.

Mathematically, the objective is to minimize the following functional

$$\mathcal{J}(u, s) = \frac{1}{2} \int_{\Omega} (s - d)^2 dx + \frac{\alpha}{2} \int_{\Omega} u^2 dx, \quad (3.1)$$

subject to

$$-\kappa \Delta s = u \quad \text{in } \Omega, \quad (3.2)$$

$$s = 0 \quad \text{on } \partial\Omega, \quad (3.3)$$

where Ω is a bounded domain, $s : \Omega \rightarrow \mathbb{R}$ is the unknown temperature satisfying equation 3.2, subject to the boundary conditions prescribed in equation 3.3. Moreover, $d : \Omega \rightarrow \mathbb{R}$ is the given desired temperature profile, while $f : \Omega \rightarrow \mathbb{R}$ is the unknown control function acting as source term. In addition, $\kappa \in \mathbb{R}$ is the thermal diffusivity, and $\alpha \geq 0$ is a Tikhonov regularization parameter, which is one of the most commonly used methods of regularization of ill-posed problems [50]. In this example, we set $\Omega = [0, 1]$, $\kappa = 1$, $\alpha = 0$, and $d(x) = \frac{1}{\pi^2} \sin(\pi x)$. Consequently, $u(x) = \sin(\pi x)$ is the global minimum at which we have $\mathcal{J} = 0$.

Following the first step of Algorithm 1, we use a DeepONet G_θ to represent the solution operator G mapping the source term u to the associated PDE solution s , where the branch network and the trunk network are two separate 5-layer modified multi-layer perceptrons (MLPs) with 100 neurons per hidden layer and hyperbolic tangent activation functions (see Appendix E for details). According to equations 3.2 - 3.3, a physics-informed loss function can be formulated as follows

$$\mathcal{L}(\theta) = \mathcal{L}_{\text{BC}}(\theta) + \mathcal{L}_{\text{PDE}}(\theta), \quad (3.4)$$

where

$$\mathcal{L}_{\text{BC}}(\theta) = \frac{1}{NP} \sum_{i=1}^N \sum_{j=1}^P \left| G_\theta(\mathbf{u}^{(i)})(y_{b,j}^{(i)}) \right|^2, \quad (3.5)$$

$$\mathcal{L}_{\text{PDE}}(\theta) = \frac{1}{NQ} \sum_{i=1}^N \sum_{j=1}^Q \left| \frac{\partial^2 G_\theta(\mathbf{u}^{(i)})(y_{r,j}^{(i)})}{\partial y^2} u^{(i)}(y_{r,j}^{(i)}) \right|^2. \quad (3.6)$$

Here, $\mathbf{u}^{(i)} = [u(x_1), u(x_2), \dots, u(x_m)]$ represents an input function evaluated at a fixed equi-spaced grid $\{x_i\}_{i=1}^m$ in $[0, 1]$. For every i , $\{y_{b,j}\}_{j=1}^P$ and $\{y_{r,j}\}_{j=1}^Q$ are uniformly sampled from the boundary $\partial\Omega$ and the computational domain Ω for enforcing the boundary condition and the PDE constraint, respectively. To generate a set of training data, we take $N = 5 \times 10^4$, $P = 2$, $Q = m = 100$ and sample N input functions $\{u^{(i)}\}_{i=1}^N$ from a Gaussian random field (GRF) with a length scale $l = 0.2$. We obtain a test data-set by sampling another $N = 10^3$ input functions from the same GRF and solving the Poisson equation using a finite difference method on a uniform grid.

We train the physics-informed DeepONet by minimizing the above loss function for 10^5 iterations of gradient descent using Adam optimizer [51]. The averaged relative L^2 error over the test data-set is 0.09%. This is consistent with the visualizations shown in Figure 8, from which an excellent agreement can be observed between the reference and the predicted solutions for different input samples in the test data-set. Then, according to step 2 in the proposed Algorithm 1, we parameterize the source term u by a 5-layer fully-connected neural network u_α with 100 neurons per hidden layer. The optimal control can be solved by minimizing the following loss function

$$\mathcal{J}(u_\alpha) = \frac{1}{2} \int_{\Omega} (G_{\theta^*}(\mathbf{u}_\alpha)(y) - d(y)) dy, \quad (3.7)$$

where G_{θ^*} denotes the trained physics-informed DeepONet and $\mathbf{u}_\alpha = [u_\alpha(x_1), u_\alpha(x_2), \dots, u_\alpha(x_m)]$ is an m -dimensional vector obtained by evaluating the network u_α at the fixed sensors $\{x_i\}_{i=1}^m$. We minimize the loss function \mathcal{J} for 2×10^5 iterations of gradient descent using the Adam optimizer. The top panel of Figure 2 presents a comparison of the learned control u against the reference optimal control. It can be observed that the learned control and the ground truth are in excellent agreement with a resulting relative L^2 error of 0.37%. Moreover, the evolution of the loss functions during training are provided in the bottom panel of Figure 2. It worth emphasizing that, given a trained physics-informed DeepONet, it takes less just a few seconds to run 2×10^5 iterations of gradient descent when training the network u_α , since the PDE solution and its gradients with respect to α can be evaluated rapidly. Notice, that α here contains all the weights and biases parametrizing the continuous control function u , thus defining a $\mathcal{O}(10^4)$ -dimensional PDE-constrained optimization task that is solved in a matter of seconds on a single graphics processing unit (GPU) (see Appendix C for a more detailed discussion on computational cost).

3.2 Optimal control of a 2D heat equation

Our next example aims to solve a optimal control problem involving time-dependent heat transfer. Specifically, we consider minimizing the following objective function

$$J(u) = \int_0^T \int_{\Omega} (s - d)^2 \, d\Omega dt + \frac{\alpha}{2} \int_0^T \int_{\Omega} \dot{u}^2 \, d\Omega dt, \quad (3.8)$$

where the second integral is a regularization term that enforces smoothness of the control in time. In particular, the time-dependent control function $u = u(t)$ satisfies

$$\frac{\partial s}{\partial t} - \nu \nabla^2 s = u \text{ in } \Omega \times (0, T) \quad (3.9)$$

$$s = 0 \text{ for } \Omega \times \{0\}, \quad (3.10)$$

$$s = 0 \text{ for } \partial\Omega \times (0, T), \quad (3.11)$$

In this example we set $T = 2$, $\nu = 0.01$, $\Omega = [0, 1]^2$ and

$$d(x, y) = 16xy(x - 1)(y - 1) \sin(\pi t). \quad (3.12)$$

Similar to the first example, we proceed by training a physics-informed DeepONet to learn the solution operator that maps source terms u to the corresponding PDE solution s . To this end, we proceed by approximating the operator by a 7-layer modified DeepONet G_θ (see Appendix B,E for details). Then, we can define the PDE residual according to equation 3.9 as

$$\mathcal{R}_\theta(\mathbf{u})(x, y, t) = \frac{\partial G_\theta(x, y, t)}{\partial t} - \nu \left(\frac{\partial^2 G_\theta(x, y, t)}{\partial x^2} + \frac{\partial^2 G_\theta(x, y, t)}{\partial y^2} \right). \quad (3.13)$$

The training loss function is given as

$$\mathcal{L}(\theta) = \mathcal{L}_{\text{IC}}(\theta) + \mathcal{L}_{\text{BC}}(\theta) + \mathcal{L}_{\text{PDE}}(\theta), \quad (3.14)$$

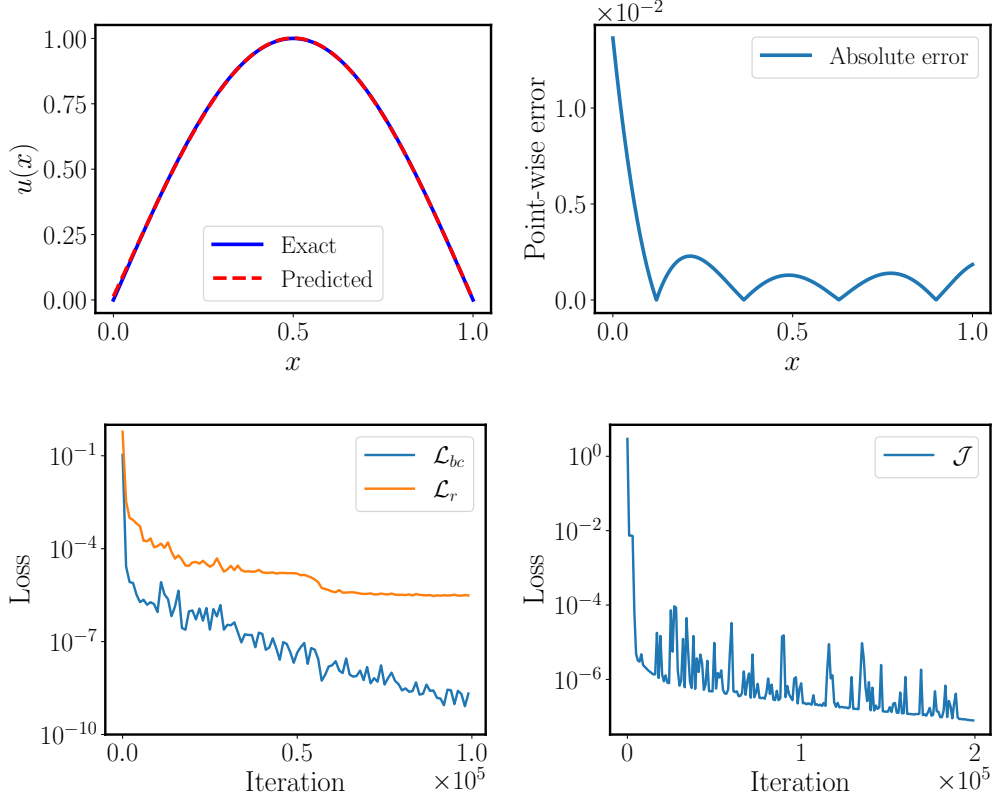


Figure 2: *Optimal control of a 1D Poisson problem: Top: Exact control versus the predicted control. The relative L^2 error is 0.37%. Bottom left: Training loss convergence of a physics-informed DeepONet for 10^5 gradient descent iterations. Bottom right: Cost functional convergence for 2×10^5 iterations.*

where

$$\mathcal{L}_{\text{IC}}(\boldsymbol{\theta}) = \frac{1}{NP} \sum_{i=1}^N \sum_{j=1}^P \left| G_{\boldsymbol{\theta}}(\mathbf{u}^{(i)})(x_{ic,j}^{(i)}, y_{ic,j}^{(i)}, t_{ic,j}^{(i)}) \right|^2, \quad (3.15)$$

$$\mathcal{L}_{\text{BC}}(\boldsymbol{\theta}) = \frac{1}{NP} \sum_{i=1}^N \sum_{j=1}^P \left| G_{\boldsymbol{\theta}}(\mathbf{u}^{(i)})(x_{bc,j}^{(i)}, y_{bc,j}^{(i)}, t_{bc,j}^{(i)}) \right|^2, \quad (3.16)$$

$$\mathcal{L}_{\text{PDE}}(\boldsymbol{\theta}) = \frac{1}{NQ} \sum_{i=1}^N \sum_{j=1}^Q \left| \mathcal{R}_{\boldsymbol{\theta}}(\mathbf{u}^{(i)})(x_{r,j}^{(i)}, y_{r,j}^{(i)}, t_{r,j}^{(i)}) - u^{(i)}(t_{r,j}^{(i)}) \right|^2. \quad (3.17)$$

Here $\mathbf{u}^{(i)} = [u(t_1), u(t_2), \dots, u(t_m)]$ denotes an input sample evaluated at a fixed uniform grid $\{t_i\}_{i=1}^m$ in $[0, 2]$. For each i , $\{x_{ic,j}^{(i)}, y_{ic,j}^{(i)}, t_{ic,j}^{(i)}\}_{j=1}^P$, and $\{x_{bc,j}^{(i)}, y_{bc,j}^{(i)}, t_{bc,j}^{(i)}\}_{j=1}^P$ are randomly sampled from $\Omega \times \{0\}$ and $\partial\Omega \times (0, T)$, respectively. In addition, $\{x_{r,j}^{(i)}, y_{r,j}^{(i)}, t_{r,j}^{(i)}\}_{j=1}^Q$ is a set of collocation points randomly selected from $\Omega \times (0, T)$ for enforcing the underlying PDE constraint. Specifically, we take $N = 10^3$ and $m = 100$, $P = Q = 100$. All input functions are sampled from a GRF with a length scale $l = 0.2$.

We train the physics-informed DeepONet by minimizing the loss of equation 3.14 for 4×10^5 iterations of gradient descent using the Adam optimizer. The resulting relative test error is 1.51% averaged over all examples in the test data-set, while the loss convergence is visualized in Figure 3 (see Appendix F.1 for more details on validation). Some visualizations of the predicted solution for different source terms are provided in Figure 9. Recall that our goal is to find the desired source term that resulting in the given temperature distribution over time. We proceed by approximating the latent function u by a 5-layer fully-connected neural network u_{α} with 100 neurons per hidden layer. Then, this optimal

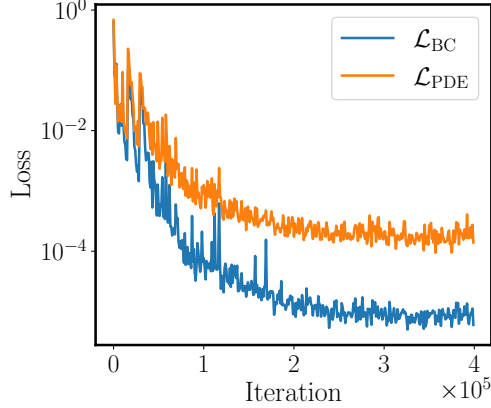


Figure 3: : *Optimal control of a 2D heat equation:* Training loss convergence of a physics-informed DeepONet for 4×10^5 iterations. Here we remark that we treat the initial condition as a special type of boundary condition, and thus \mathcal{L}_{IC} is absorbed in \mathcal{L}_{BC} .

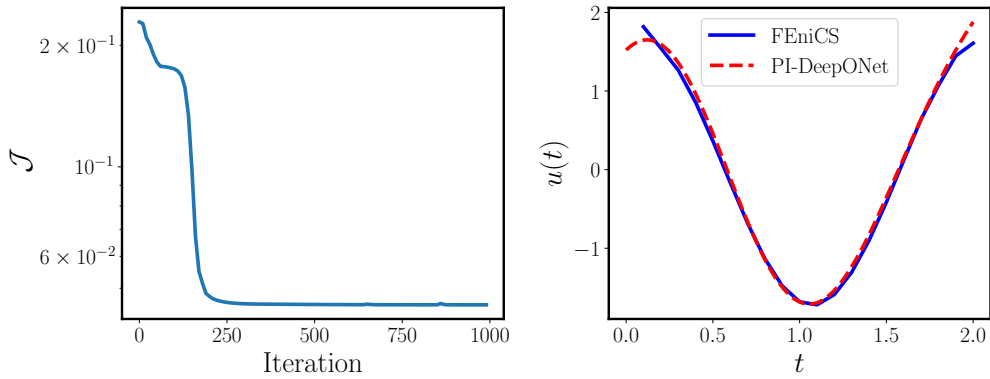


Figure 4: : *Optimal control of a 2D heat equation:* *Left:* Training cost convergence for 10^3 iterations. *Right:* Inferred control function versus the baseline solution obtained using the FEniCS finite element solver. The relative L^2 error is 7.44%. An animation of the control optimization process is provided at <https://github.com/PredictiveIntelligenceLab/PDE-constrained-optimization-PI-DeepONet/tree/main/animations/heat>.

control task be solved by minimizing the following cost functional

$$\mathcal{J}(u_\alpha) = \int_0^T \int_\Omega (G_{\theta^*})(\mathbf{u}_\alpha) - d) d\Omega dt, \quad (3.18)$$

where G_{θ^*} denotes the trained physics-informed DeepONet, and $\mathbf{u}_\alpha = [u_\alpha(t_1), u_\alpha(t_2), \dots, u_\alpha(t_m)]$ is an m -dimensional vector evaluated at the fixed sensors $\{t_i\}_{i=1}^m$. It is worth noting that we take $\alpha = 0$ in equation 3.8 since the smoothness is implicitly guaranteed by the assumed neural network parametrization for $u(t)$, and therefore the regularization term is not needed. We train the network u_α by minimizing the above cost function \mathcal{J} for 1,000 iterations. As shown in Figure 4 and Figure 5, the objective function rapidly converges after the first few hundred iterations and the total computation cost is 25 seconds, which is 5x faster than a conventional adjoint method using the finite element solver FEniCS [52] (see Appendix C for a more detailed discussion on computational cost). A visual assessment of the learned control is presented in the right panel of Figure 4, indicated that the inferred control function achieves a good agreement with the reference solution, although some discrepancies can be observed near the two end points. This may be because, in the case of the adjoint finite element solver, the control function is parametrized by a vector of 100 discrete values, whereas in the proposed deep learning approach, the control function is a smooth continuous function parametrized by an MLP network with $\mathcal{O}(10^4)$ trainable parameters.

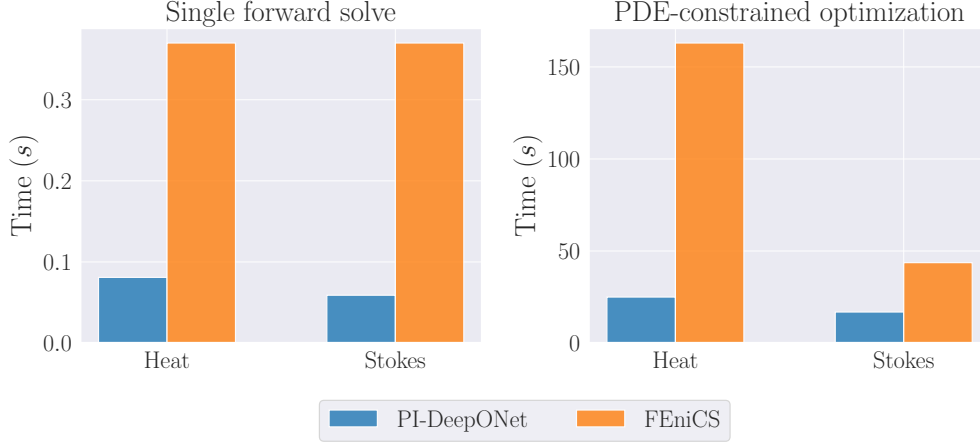


Figure 5: *Computational cost*: *Left*: Computational cost (sec) for performing inference with a trained physics-informed DeepONet model, versus solving a single PDE instance (for the 2D heat equation and Stokes flow, respectively) with the FEniCS finite element solver. *Right*: Training time (sec) of performing PDE-constrained optimization via the trained physics-informed DeepONet, versus a baseline adjoint method using FEniCS.

3.3 Drag minimization of obstacles in Stokes-flow

To demonstrate the capability of the proposed algorithm to perform shape optimization, our last example considers minimizing the drag of a bluff body subject to Stokes flow. The goal is to determine the shape of an obstacle Γ , which minimizes the dissipated power in the fluid. More specifically, the cost function \mathcal{J} is described as follows

$$\mathcal{J}(\Gamma, \mathbf{u}) = \mathcal{J}_D(\Gamma) + \alpha \mathcal{J}_V(\Gamma) + \beta \mathcal{J}_B(\Gamma) \quad (3.19)$$

$$= \int_{\Omega/\Gamma} \left(\frac{\partial u}{\partial x} \right)^2 + \left(\frac{\partial u}{\partial y} \right)^2 + \left(\frac{\partial v}{\partial x} \right)^2 + \left(\frac{\partial v}{\partial y} \right)^2 dx dy \quad (3.20)$$

$$+ \alpha |\text{Vol}(\Gamma) - \text{Vol}(\Gamma_0)|^2 \quad (3.21)$$

$$+ \beta \sum_{j=1}^2 |\text{Bc}_j(\Gamma) - \text{Bc}_j(\Gamma_0)|^2, \quad (3.22)$$

where $\Omega = [0, 1] \times [0, 1]$ denotes the computational domain, Γ_0 denotes the obstacle boundary, and $\text{Vol}(\Gamma)$ and $\text{Bc}_j(\Gamma)$ is the volume and j -th component of the barycenter of the obstacle, respectively. In particular, $\mathbf{u} = (u, v)$ represents a velocity field subject to the Stokes equations

$$-\Delta \mathbf{u} + \nabla p = 0, \quad (x, y) \in \Omega/\Gamma, \quad (3.23)$$

$$\nabla \cdot \mathbf{u} = 0, \quad (x, y) \in \Omega/\Gamma, \quad (3.24)$$

subject to boundary conditions

$$\mathbf{u} = \mathbf{0}, \quad (x, y) \in \Lambda_1 \cup \partial\Gamma, \quad (3.25)$$

$$\mathbf{u} = \mathbf{g}, \quad (x, y) \in \Lambda_2 \quad (3.26)$$

$$p = 0, \quad (x, y) \in \Lambda_3, \quad (3.27)$$

where Λ_1 denotes wall boundaries, while Λ_2 and Λ_3 correspond to the inlet and the outlet of a 2D channel, respectively.

In this example, we parametrize the shape of the obstacle Γ by a family of ellipsoids centered at $(\frac{1}{2}, \frac{1}{2})$, i.e.

$$\partial\Gamma = \partial\Gamma(\phi) = \left(a \cos(\phi) + \frac{1}{2}, b \sin(\phi) + \frac{1}{2} \right), \quad \phi \in [0, 2\pi), \quad (3.28)$$

where $a, b > 0$ denote the length of the long or the short axis. Specifically, the shape of Γ_0 is initialized as a circle with radius $r = 0.12$. Note that an ellipse Γ is symmetric and its volume can be simply computed by $\text{Vol}(\Gamma) = \pi ab$. Consequently $\mathcal{J}_B = 0$, and then we can exactly enforce the volume constraint \mathcal{J}_V by setting $b = \frac{\text{Vol}(\Gamma_0)}{\pi a}$. As such, the cost functional function for the dissipated power can be written as

$$\mathcal{J}(\Gamma) = \mathcal{J}(a) = \int_{\Omega/\Gamma} \left(\frac{\partial u}{\partial x} \right)^2 + \left(\frac{\partial u}{\partial y} \right)^2 + \left(\frac{\partial v}{\partial x} \right)^2 + \left(\frac{\partial v}{\partial y} \right)^2 dx dy, \quad (3.29)$$

where

$$\partial\Gamma = \partial\Gamma(\phi) = (a \cos(\phi) + \frac{1}{2}, \frac{\text{Vol}(\Gamma_0)}{\pi a} \sin(\phi) + \frac{1}{2}), \quad \phi \in [0, 2\pi]. \quad (3.30)$$

To represent the solution operator G that maps different obstacle geometries to the associated Stokes flow solution, we employ a 7-layer modified DeepONet architecture G_θ with 100 neurons per hidden layer and with 3-dimensional vector-valued outputs for representing u, v, p respectively, i.e.,

$$\partial\Gamma \xrightarrow{G_\theta} [G_\theta^{(u)}, G_\theta^{(v)}, G_\theta^{(p)}]. \quad (3.31)$$

Then, we can define the following PDE residuals

$$\mathcal{R}_\theta^{(1)}(\partial\Gamma)(x, y) = -\frac{\partial^2 G_\theta^{(u)}(\partial\Gamma)(x, y)}{\partial x^2} - \frac{\partial^2 G_\theta^{(u)}(\partial\Gamma)(x, y)}{\partial y^2} + \frac{\partial G_\theta^{(p)}(\partial\Gamma)(x, y)}{\partial x}, \quad (3.32)$$

$$\mathcal{R}_\theta^{(2)}(\partial\Gamma)(x, y) = -\frac{\partial^2 G_\theta^{(v)}(\partial\Gamma)(x, y)}{\partial x^2} - \frac{\partial^2 G_\theta^{(v)}(\partial\Gamma)(x, y)}{\partial y^2} + \frac{\partial G_\theta^{(p)}(\partial\Gamma)(x, y)}{\partial y}, \quad (3.33)$$

$$\mathcal{R}_\theta^{(3)}(\partial\Gamma)(x, y) = \frac{\partial G_\theta^{(u)}(\partial\Gamma)(x, y)}{\partial x} + \frac{\partial G_\theta^{(v)}(\partial\Gamma)(x, y)}{\partial y}, \quad (3.34)$$

where $\partial\Gamma = [\partial\Gamma(\phi_1), \partial\Gamma(\phi_2), \dots, \partial\Gamma(\phi_m)]$ denotes an input closed curve evaluated at evenly-spaced grid points $\{\phi\}_{i=1}^m$ in $[0, 2\pi]$. Then, a physics-informed DeepONet can be trained by minimizing the following weighted loss function

$$\mathcal{L}(\theta) = \sum_{k=1}^3 \lambda_{\text{BC}}^{(k)} \mathcal{L}_{\text{BC}}^{(k)}(\theta) + \sum_{k=1}^3 \lambda_{\text{PDE}}^{(k)} \mathcal{L}_{\text{PDE}}^{(k)}(\theta), \quad (3.35)$$

where $\{\lambda_{\text{BC}}^{(k)}\}_{k=1}^3$ and $\{\lambda_{\text{PDE}}^{(k)}\}_{k=1}^3$ are some hyper-parameters that calibrate the learning rate of each term contributing to the total loss $\mathcal{L}(\theta)$. In practice, we update these hyper-parameters using the adaptive NTK-guided weight algorithm put forth by Wang *et al.* [45] at each iteration during training. Particularly,

$$\mathcal{L}_{\text{BC}}^{(1)}(\theta) = \frac{1}{NP} \sum_{i=1}^N \sum_{j=1}^P \left[\left| G_\theta^{(u)}(\partial\Gamma^{(i)})(x_{\text{bc}1,j}^{(i)}, y_{\text{bc}1,j}^{(i)}) \right|^2 + \left| G_\theta^{(v)}(\partial\Gamma^{(i)})(x_{\text{bc}1,j}^{(i)}, y_{\text{bc}1,j}^{(i)}) \right|^2 \right], \quad (3.36)$$

$$\mathcal{L}_{\text{BC}}^{(2)}(\theta) = \frac{1}{NP} \sum_{i=1}^N \sum_{j=1}^P \left[\left| G_\theta^{(u)}(\partial\Gamma^{(i)})(x_{\text{bc}2,j}^{(i)}, y_{\text{bc}2,j}^{(i)}) - \sin(\pi y_{\text{bc}2,j}^{(i)}) \right|^2 + \left| G_\theta^{(v)}(\partial\Gamma^{(i)})(x_{\text{bc}2,j}^{(i)}, y_{\text{bc}2,j}^{(i)}) \right|^2 \right], \quad (3.37)$$

$$\mathcal{L}_{\text{BC}}^{(3)}(\theta) = \frac{1}{NP} \sum_{i=1}^N \sum_{j=1}^P \left| G_\theta^{(p)}(\partial\Gamma^{(i)})(x_{\text{bc}3,j}^{(i)}, y_{\text{bc}3,j}^{(i)}) \right|^2, \quad (3.38)$$

and

$$\mathcal{L}_{\text{PDE}}^{(k)}(\theta) = \frac{1}{NQ} \sum_{i=1}^N \sum_{j=1}^Q \left| \mathcal{R}_\theta^{(k)}(\partial\Gamma^{(i)})(x_{r,j}^{(i)}, y_{r,j}^{(i)}) \right|^2, \quad k = 1, 2, 3. \quad (3.39)$$

Here, for each input sample $\partial\Gamma^{(i)}$, $\{x_{\text{bc}1,j}^{(i)}, y_{\text{bc}1,j}^{(i)}\}_{j=1}^P$, $\{x_{\text{bc}2,j}^{(i)}, y_{\text{bc}2,j}^{(i)}\}_{j=1}^P$, $\{x_{\text{bc}3,j}^{(i)}, y_{\text{bc}3,j}^{(i)}\}_{j=1}^P$ and $\{x_{r,j}^{(i)}, y_{r,j}^{(i)}\}_{j=1}^Q$ are uniformly sampled at the boundaries $\Lambda_1 \cup \partial\Gamma$, Λ_2 , Λ_3 and inside the domain Ω/Γ , respectively. In this example, we set $N = 1000$, $m = P = 100$, $Q = 2500$. To prepare the training data-set, we randomly sample a, b from a uniform distribution $\mathcal{U}(0.05, 0.3)$, and obtain a set of input curves $\{\partial\Gamma^{(i)}\}_{i=1}^N$ using equation (3.28). To generate a set of test data, we repeat the same procedure to obtain 500 new curves, and obtain the corresponding PDE solutions using the FEniCS solver [52] (see validation details in Appendix F.2).

We train the physics-informed DeepONet for 3×10^5 iterations of gradient descent using the Adam optimizer. The loss curves and the resulting test error are shown in Figure 6 and Table 1, respectively. Moreover, some visualizations of the predicted solution across different obstacle shapes are provided in Figure 10 - 12. From these results, one may conclude that the trained physics-informed DeepONet approximates the solution operator with sufficient accuracy.

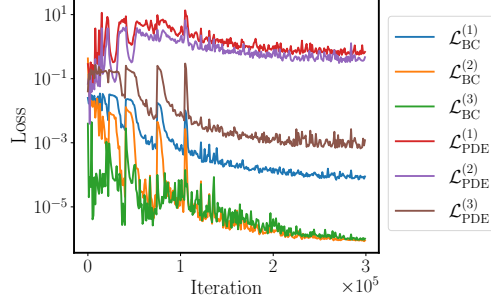


Figure 6: : Drag minimization of obstacles in Stokes-flow: Training loss convergence of a physics-informed DeepONet for 3×10^5 iterations.

Latent variable	u	v	p
Test error	$0.97\% \pm 0.24\%$	$4.79\% \pm 0.53\%$	$1.53\% \pm 0.67\%$

Table 1: : Drag minimization of obstacles in Stokes-flow: Test error of the predicted velocity and pressure field obtained from a trained physics-informed DeepONet.

Next, we can employ the trained physics-informed DeepONet to expediently minimize the cost functional of equation 3.29 as

$$\mathcal{J}(a) = \int_{\Omega/\Gamma} \left(\frac{\partial G_{\theta^*}^{(u)}(\partial\Gamma)(x, y)}{\partial x} \right)^2 + \left(\frac{\partial G_{\theta^*}^{(u)}(\partial\Gamma)(x, y)}{\partial y} \right)^2 \quad (3.40)$$

$$+ \left(\frac{\partial G_{\theta^*}^{(v)}(\partial\Gamma)(x, y)}{\partial x} \right)^2 + \left(\frac{\partial G_{\theta^*}^{(v)}(\partial\Gamma)(x, y)}{\partial y} \right)^2 \text{ dx dy}, \quad (3.41)$$

where G_{θ^*} denotes the trained physics-informed DeepONet. Notice here that parametrized the obstacle shape $\partial\Gamma = [\partial\Gamma(\phi_1), \partial\Gamma(\phi_2), \dots, \partial\Gamma(\phi_m)]$ using $m = 100$ evenly-spaced grid points $\{\phi\}_{i=1}^m$ in $[0, 2\pi]$. It is also worth noting that all gradients required to evaluate the above cost functional and its derivatives can be computed via automatic differentiation.

The left panel of Figure 7 shows the convergence of the cost functional during minimization via gradient descent. We can see that $\mathcal{J}(a)$ decreases rapidly and converges to a local minimum within a few hundred iterations. Moreover, the overall optimization time takes less than 20s, which is noticeably faster than employing an adjoint finite element solver as a forward model in this loop, see figure 5. From the right panel of Figure 7, the predicted optimal obstacle achieves an excellent agreement with the reference solution, with a resulting relative error of 0.51% (see Appendix F.2 for more details on validation). Finally, we remark that a DeepONet with a conventional architecture [46] may not be able to solve this control problem, since the cost functional requires the gradients of the predicted velocity field, which are possibly inaccurate as discussed in Wang *et al.* [37].

4 Discussion

We presented a self-supervised deep learning framework that enables the construction of fast and differentiable surrogates for solving parametric PDEs, and illustrated its effectiveness in tackling high-dimensional PDE-constrained optimization problems. The proposed physics-informed DeepONet surrogates can be trained in the absence of paired input-output data, and therefore do not require one to generate large training data-sets by repeatedly evaluating expensive simulators or experiments, as is typically the case for building reduced order models. We examined and validated the effectiveness of the proposed framework through a series of numerical experiments involving time-distributed optimal control of heat transfer, and drag minimization of Stokes flow over obstacles. Our findings suggest that the proposed is not only capable of handling continuous, infinite-dimensional control functions, but also is notably faster than conventional adjoint solvers with comparable predictive accuracy. Given the prominence of PDE-constrained optimization problems across all corners of science and engineering, we expect that this work can have a broad technical impact in accelerating the design and control of complex systems.

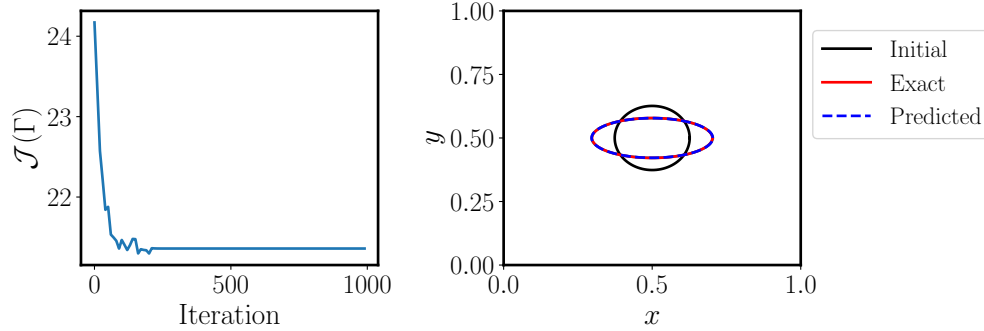


Figure 7: *Drag minimization of obstacles in Stokes-flow: Left: Convergence of the target cost functional for 10^3 gradient descent iterations. Right: Learned optimal obstacle geometry versus the reference solution obtained by the adjoint finite element solver FEniCS. The relative L^2 error is 0.51%. An animation of the shape optimization process can be found in <https://github.com/PredictiveIntelligenceLab/PDE-constrained-optimization-PI-DeepONet/tree/main/animations/Stokes>.*

Currently the main roadblock for scaling the proposed techniques to more realistic applications is the ability of physics-informed neural networks and physics-informed DeepONets to accurately solve more complex PDEs involving multi-scale solutions, stiff dynamics, and large spatio-temporal domains. Issues including spectral bias [43], ill-conditioned loss landscapes [53], and gradient pathologies [41], pose practical difficulties in training physics-informed deep learning models in these more challenging settings. Although progress is being made [42, 45], we are still in the early stages of demystifying how physics-informed deep learning models can be a reliable and effective tool for emulating complex PDEs in the absence of labelled training data. To this end, designing more effective neural network architectures, initialization schemes and optimizers will be the key to unlocking the full potential of physics-informed DeepONets in enabling the real-time solution of more realistic PDE-constrained optimization problems, and beyond.

Acknowledgments

This work received support from DOE grant DE-SC0019116, AFOSR grant FA9550-20-1-0060, and DOE-ARPA grant DE-AR0001201. We would also like to thank the developers of the software that enabled our research, including JAX [54], Matplotlib [55], NumPy [56], FEniCS [52], and dolfin-adjoint [57].

Competing Interests

The authors declare that they have no competing interests.

Author Contributions

SW and PP conceptualized the research and designed the numerical studies. SW implemented the methods and conducted the numerical experiments. MAB assisted with the numerical studies and generated the validation data-sets. PP provided funding and supervised all aspects of this work. SW, MAB and PP wrote the manuscript.

Data and materials availability

All methods needed to evaluate the conclusions in the paper are present in the paper and/or the Appendix. All code and data accompanying this manuscript will be made publicly available at <https://github.com/PredictiveIntelligenceLab/PDE-constrained-optimization-PI-DeepONet>.

References

- [1] Jan Sokolowski and Jean-Paul Zolésio. Introduction to shape optimization. In *Introduction to shape optimization*, pages 5–12. Springer, 1992.

- [2] Jaroslav Haslinger and Raino AE Mäkinen. *Introduction to shape optimization: theory, approximation, and computation*. SIAM, 2003.
- [3] Frank L Lewis, Draguna Vrabie, and Vassilis L Syrmos. *Optimal control*. John Wiley & Sons, 2012.
- [4] Juan Carlos De los Reyes and Carola-Bibiane Schönlieb. Image denoising: learning the noise model via nonsmooth pde-constrained optimization. *Inverse Problems & Imaging*, 7(4):1183, 2013.
- [5] Raymond M Hicks and Preston A Henne. Wing design by numerical optimization. *Journal of Aircraft*, 15(7):407–412, 1978.
- [6] Paul D Frank and Gregory R Shubin. A comparison of optimization-based approaches for a model computational aerodynamics design problem. *Journal of Computational Physics*, 98(1):74–89, 1992.
- [7] James Ng and Stevan Džurđević. Optimal boundary control of a diffusion–convection–reaction PDE model with time-dependent spatial domain: Czochralski crystal growth process. *Chemical engineering science*, 67(1):111–119, 2012.
- [8] Siddhartha P Chakrabarty and Floyd B Hanson. Optimal control of drug delivery to brain tumors for a distributed parameters model. In *Proceedings of the 2005, American Control Conference, 2005.*, pages 973–978. IEEE, 2005.
- [9] Giampietro Fabbri. Heat transfer optimization in corrugated wall channels. *International Journal of Heat and Mass Transfer*, 43(23):4299–4310, 2000.
- [10] Qun Chen, Moran Wang, Ning Pan, and Zeng-Yuan Guo. Optimization principles for convective heat transfer. *Energy*, 34(9):1199–1206, 2009.
- [11] Gerard Cornuejols and Reha Tütüncü. *Optimization methods in finance*, volume 5. Cambridge University Press, 2006.
- [12] Charles Audet, J Denni, Douglas Moore, Andrew Booker, and Paul Frank. A surrogate-model-based method for constrained optimization. In *8th symposium on multidisciplinary analysis and optimization*, page 4891, 2000.
- [13] Nestor V Queipo, Raphael T Haftka, Wei Shyy, Tushar Goel, Rajkumar Vaidyanathan, and P Kevin Tucker. Surrogate-based analysis and optimization. *Progress in aerospace sciences*, 41(1):1–28, 2005.
- [14] Alexander IJ Forrester and Andy J Keane. Recent advances in surrogate-based optimization. *Progress in aerospace sciences*, 45(1-3):50–79, 2009.
- [15] Graeme J Kennedy and Joaquim RRA Martins. A parallel finite-element framework for large-scale gradient-based design optimization of high-performance structures. *Finite Elements in Analysis and Design*, 87:56–73, 2014.
- [16] Alex Beatson, Jordan Ash, Geoffrey Roeder, Tianju Xue, and Ryan Adams. Learning composable energy surrogates for PDE order reduction. In *Advances in neural information processing systems*, 2020.
- [17] Tianju Xue, Alex Beatson, Sigrid Adriaenssens, and Ryan Adams. Amortized finite element analysis for fast PDE-constrained optimization. In *37th International Conference on Machine Learning*, pages 10638–10647. PMLR, 2020.
- [18] Elizabeth G Ryan, Christopher C Drovandi, James M McGree, and Anthony N Pettitt. A review of modern computational algorithms for Bayesian optimal design. *International Statistical Review*, 84(1):128–154, 2016.
- [19] Rémi Lam, Matthias Poloczek, Peter Frazier, and Karen E Willcox. Advances in Bayesian optimization with applications in aerospace engineering. In *2018 AIAA Non-Deterministic Approaches Conference*, page 1656, 2018.
- [20] David J Lucia, Philip S Beran, and Walter A Silva. Reduced-order modeling: new approaches for computational physics. *Progress in aerospace sciences*, 40(1-2):51–117, 2004.
- [21] Alfio Quarteroni, Gianluigi Rozza, et al. *Reduced order methods for modeling and computational reduction*, volume 9. Springer, 2014.
- [22] Lawrence Sirovich. Turbulence and the dynamics of coherent structures. i. coherent structures. *Quarterly of applied mathematics*, 45(3):561–571, 1987.
- [23] Karen Willcox and Jaime Peraire. Balanced model reduction via the proper orthogonal decomposition. *AIAA journal*, 40(11):2323–2330, 2002.
- [24] C Audouze, F De Vuyst, and PB Nair. Reduced-order modeling of parameterized PDEs using time–space–parameter principal component analysis. *International journal for numerical methods in engineering*, 80(8):1025–1057, 2009.
- [25] Ronald R Coifman, Ioannis G Kevrekidis, Stéphane Lafon, Mauro Maggioni, and Boaz Nadler. Diffusion maps, reduction coordinates, and low dimensional representation of stochastic systems. *Multiscale Modeling & Simulation*, 7(2):842–864, 2008.

- [26] Kookjin Lee and Kevin T Carlberg. Model reduction of dynamical systems on nonlinear manifolds using deep convolutional autoencoders. *Journal of Computational Physics*, 404:108973, 2020.
- [27] Romit Maulik, Bethany Lusch, and Prasanna Balaprakash. Reduced-order modeling of advection-dominated systems with recurrent neural networks and convolutional autoencoders. *Physics of Fluids*, 33(3):037106, 2021.
- [28] Jiayang Xu and Karthik Duraisamy. Multi-level convolutional autoencoder networks for parametric prediction of spatio-temporal dynamics. *Computer Methods in Applied Mechanics and Engineering*, 372:113379, 2020.
- [29] Roland Herzog and Karl Kunisch. Algorithms for PDE constrained optimization. *GAMM-Mitteilungen*, 33(2):163–176A3081, 2010.
- [30] David Amsallem and Charbel Farhat. Interpolation method for adapting reduced-order models and application to aeroelasticity. *AIAA journal*, 46(7):1803–1813, 2008.
- [31] Lorenz T Biegler, Omar Ghattas, Matthias Heinkenschloss, David Keyes, and Bart van Bloemen Waanders. *Real-time PDE-constrained Optimization*. SIAM, 2007.
- [32] Hidenori Sasaki and Hajime Igarashi. Topology optimization accelerated by deep learning. *IEEE Transactions on Magnetism*, 55(6):1–5, 2019.
- [33] Sunae So, Trevon Badloe, Jaebum Noh, Jorge Bravo-Abad, and Junsuk Rho. Deep learning enabled inverse design in nanophotonics. *Nanophotonics*, 9(5):1041–1057, 2020.
- [34] Kai Guo, Zhenze Yang, Chi-Hua Yu, and Markus J Buehler. Artificial intelligence and machine learning in design of mechanical materials. *Materials Horizons*, 8(4):1153–1172, 2021.
- [35] Stephan Hoyer, Jascha Sohl-Dickstein, and Sam Greydanus. Neural reparameterization improves structural optimization. *arXiv preprint arXiv:1909.04240*, 2019.
- [36] Somil Bansal and Claire J Tomlin. Deepreach: A deep learning approach to high-dimensional reachability. In *2021 IEEE International Conference on Robotics and Automation (ICRA)*, pages 1817–1824. IEEE, 2021.
- [37] Sifan Wang, Hanwen Wang, and Paris Perdikaris. Learning the solution operator of parametric partial differential equations with physics-informed DeepOnets. *arXiv preprint arXiv:2103.10974*, 2021.
- [38] Maziar Raissi, Hessam Babaei, and Peyman Givi. Deep learning of turbulent scalar mixing. *Physical Review Fluids*, 4(12):124501, 2019.
- [39] Lu Lu, Raphael Pestourie, Wenjie Yao, Zhicheng Wang, Francesc Verdugo, and Steven G Johnson. Physics-informed neural networks with hard constraints for inverse design. *arXiv preprint arXiv:2102.04626*, 2021.
- [40] Oliver Hennigh, Susheela Narasimhan, Mohammad Amin Nabian, Akshay Subramaniam, Kaustubh Tangsali, Zhiwei Fang, Max Rietmann, Wonmin Byeon, and Sanjay Choudhry. Nvidia simnet™: An ai-accelerated multi-physics simulation framework. In *International Conference on Computational Science*, pages 447–461. Springer, 2021.
- [41] Sifan Wang, Yujun Teng, and Paris Perdikaris. Understanding and mitigating gradient flow pathologies in physics-informed neural networks. *SIAM Journal on Scientific Computing*, 43(5):A3055–A3081, 2021.
- [42] Sifan Wang, Xinling Yu, and Paris Perdikaris. When and why PINNs fail to train: A neural tangent kernel perspective. *arXiv preprint arXiv:2007.14527*, 2020.
- [43] Sifan Wang, Hanwen Wang, and Paris Perdikaris. On the eigenvector bias of fourier feature networks: From regression to solving multi-scale pdes with physics-informed neural networks. *Computer Methods in Applied Mechanics and Engineering*, 384:113938, 2021.
- [44] Sifan Wang and Paris Perdikaris. Long-time integration of parametric evolution equations with physics-informed deeponets. *arXiv preprint arXiv:2106.05384*, 2021.
- [45] Sifan Wang, Hanwen Wang, and Paris Perdikaris. Improved architectures and training algorithms for deep operator networks. *arXiv preprint arXiv:2110.01654*, 2021.
- [46] Lu Lu, Pengzhan Jin, Guofei Pang, Zhongqiang Zhang, and George Em Karniadakis. Learning nonlinear operators via DeepONet based on the universal approximation theorem of operators. *Nature Machine Intelligence*, 3(3):218–229, 2021.
- [47] Tianping Chen and Hong Chen. Universal approximation to nonlinear operators by neural networks with arbitrary activation functions and its application to dynamical systems. *IEEE Transactions on Neural Networks*, 6(4):911–917, 1995.
- [48] Andreas Griewank et al. On automatic differentiation. *Mathematical Programming: recent developments and applications*, 6(6):83–107, 1989.

- [49] Atilim Gunes Baydin, Barak A Pearlmutter, Alexey Andreyevich Radul, and Jeffrey Mark Siskind. Automatic differentiation in machine learning: a survey. *Journal of machine learning research*, 18, 2018.
- [50] Curtis R Vogel. *Computational methods for inverse problems*. SIAM, 2002.
- [51] Diederik P Kingma and Jimmy Ba. Adam: A method for stochastic optimization. *arXiv preprint arXiv:1412.6980*, 2014.
- [52] Martin Alnæs, Jan Blechta, Johan Hake, August Johansson, Benjamin Kehlet, Anders Logg, Chris Richardson, Johannes Ring, Marie E Rognes, and Garth N Wells. The fenics project version 1.5. *Archive of Numerical Software*, 3(100), 2015.
- [53] Aditi S Krishnapriyan, Amir Gholami, Shandian Zhe, Robert M Kirby, and Michael W Mahoney. Characterizing possible failure modes in physics-informed neural networks. *arXiv preprint arXiv:2109.01050*, 2021.
- [54] James Bradbury, Roy Frostig, Peter Hawkins, Matthew James Johnson, Chris Leary, Dougal Maclaurin, George Necula, Adam Paszke, Jake VanderPlas, Skye Wanderman-Milne, and Qiao Zhang. JAX: composable transformations of Python+NumPy programs, 2018.
- [55] John D Hunter. Matplotlib: A 2D graphics environment. *IEEE Annals of the History of Computing*, 9(03):90–95, 2007.
- [56] Charles R Harris, K Jarrod Millman, Stéfan J van der Walt, Ralf Gommers, Pauli Virtanen, David Cournapeau, Eric Wieser, Julian Taylor, Sebastian Berg, Nathaniel J Smith, et al. Array programming with numpy. *Nature*, 585(7825):357–362, 2020.
- [57] Sebastian K Mitusch, Simon W Funke, and Jørgen S Dokken. dolfin-adjoint 2018.1: automated adjoints for fenics and firedrake. *Journal of Open Source Software*, 4(38):1292, 2019.
- [58] Xavier Glorot and Yoshua Bengio. Understanding the difficulty of training deep feedforward neural networks. In *Proceedings of the thirteenth international conference on artificial intelligence and statistics*, pages 249–256, 2010.
- [59] Simon W. Funke and Patrick E. Farrell. A framework for automated pde-constrained optimisation. *arXiv preprint arXiv:1302.3894*, 2013.
- [60] Sebastian K. Mitusch, Simon W. Funke, and Jørrgen S. Dokken. dolfin-adjoint 2018.1: automated adjoints for fenicsand firedrake. *Journal of Open Source Software*, 4(38), 2019.
- [61] Volker Schulz and Martin Siebenborn. The Korteweg-de Vries equation: a historical essay. *Computational Methods in Applied Mathematics*, 16(3):485–496, 2016.
- [62] Jørgen S. Dokken, Sebastian K. Mitusch, and Simon W. Funke. Automatic shape derivatives for transient pdes in fenics and firedrake. *arXiv preprint arXiv:2001.10058*, 2020.
- [63] Olivier Pironneau. On optimum design in fluid mechanics. *Journal of Fluid Mechanics*, 64(1):97–110, 1974.

A Nomenclature

Table 2 summarizes the main symbols and notation used in this work.

Notation	Description
\mathcal{J}	cost function of the PDE-constrained optimization
\mathcal{N}	differential operator
\mathcal{B}	boundary condition of a PDE system
$\mathbf{u}(\cdot)$	an input function
$\mathbf{s}(\cdot)$	a solution to a parametric PDE
G	an operator
G_θ	a DeepONet representation of the operator G
u_α	a fully-connected neural network representation of the control
θ	all trainable parameters of a DeepONet
α	all trainable parameters of a control representation
$\{\mathbf{x}_i\}_{i=1}^m$	m sensor points where input functions $\mathbf{u}(\mathbf{x})$ are evaluated
$[u(\mathbf{x}_1), u(\mathbf{x}_2), \dots, u(\mathbf{x}_m)]$	an input of the branch net, representing the input function u
\mathbf{y}	an input of the trunk net, a point in the domain of $G(u)$
N	number of input samples in the training data-set
m	number of locations for evaluating the input functions u
P	number of locations for evaluating the output functions $G(u)$
Q	number of collocation points for evaluating the PDE residual
MLP	Multi-Layer Perceptron
GRF	a Gaussian random field
l	length scale of a Gaussian random field

Table 2: *Nomenclature*: Summary of the main symbols and notation used in this work.

B Hyper-parameter settings

Case	Input function space	m	P	Q	# u Train	# u Test	Iterations
1D Poisson equation	GRF($l = 0.2$)	10^2	2	10^2	10^4	10^3	10^5
2D Heat equation	GRF($l = 0.5$)	10^2	10^2	2×10^3	10^3	10^2	4×10^5
Stokes flow	Ellipse	10^2	10^2	2×10^3	10^3	10^2	3×10^5

Table 3: Default hyper-parameter settings for training physics-informed DeepONets in each benchmark (unless otherwise stated).

Case	Architecture	Trunk depth	Trunk width	Branch depth	Branch width
1D Poisson equation	Modified DeepONet	5	10^2	5	10^2
2D Heat equation	Modified DeepONet	7	10^2	7	10^2
Stokes flow	Modified DeepONet	7	10^2	7	10^2

Table 4: Physics-informed DeepONet architectures for each benchmark employed in this work (unless otherwise stated). The details of the Modified DeepONet architecture are provided in E.

Case	Architecture	Depth	Width	Iterations
1D Poisson equation	MLP	5	10^2	2×10^5
2D Heat equation	MLP	5	10^2	10^3
Stokes flow	-	-	-	10^3

Table 5: Neural network architectures for representing the control variables in each benchmark (unless otherwise stated).

C Computational cost

Case	Training time (hours)
1D Poisson equation	0.32
2D Heat equation	22.38
Stokes flow	30.12

Table 6: Computational cost (hours) for training physics-informed DeepONet models across the different benchmarks. Reported timings are obtained on a single NVIDIA RTX A6000 graphics card.

D Training procedure and error metric

Throughout all benchmarks we employ hyperbolic tangent activation functions (Tanh) and initialize the DeepONet networks using the Glorot normal scheme [58], unless otherwise stated. All networks are trained via mini-batch stochastic gradient descent using the Adam optimizer [51] with default settings. Particularly, we set the batch size to be 10,000 and use exponential learning rate decay with a decay-rate of 0.9 every 2,000 training iterations. Moreover, we employ a modified DeepONet architecture for representing the solution operator [45], which is empirically proved to perform better than the conventional DeepONet architecture. The forward pass of this architecture is illustrated in Appendix E. For the Poisson and Stokes benchmarks, an NTK-guided weighting scheme is used for training physics-informed DeepONets, see [45] for more details.

The error metric employed throughout all numerical experiments to assess model performance is the relative L^2 norm. Specifically, the reported test errors correspond to the mean of the relative L^2 error of a trained model over all examples in the test data-set, i.e

$$\text{Test error} := \frac{1}{N} \sum_{i=1}^N \frac{\|G_{\theta}(\mathbf{u}^{(i)})(y) - G(\mathbf{u}^{(i)})(y)\|_2}{\|G(\mathbf{u}^{(i)})(y)\|_2}, \quad (\text{D.1})$$

where N denotes the number of examples in the test data-set and y is typically a set of equi-spaced points in the domain of $G(u)$. Here $G_{\theta}(\mathbf{u}^{(i)})(\cdot)$ denotes a predicted DeepONet output function, while $G(\mathbf{u}^{(i)})(\cdot)$ corresponds to the ground truth target functions.

E Modified DeepONet architecture

The forward pass of a L -layer modified DeepONet architecture [45] is given as follows

$$\mathbf{U} = \phi(\mathbf{W}_u \mathbf{u} + \mathbf{b}_u), \quad \mathbf{V} = \phi(\mathbf{W}_y \mathbf{y} + \mathbf{b}_y) \quad (\text{E.1})$$

$$\mathbf{H}_u^{(1)} = \phi(\mathbf{W}_u^{(1)} \mathbf{u} + \mathbf{b}_u^{(1)}), \quad \mathbf{H}_y^{(1)} = \phi(\mathbf{W}_y^{(1)} \mathbf{y} + \mathbf{b}_y^{(1)}) \quad (\text{E.2})$$

$$\mathbf{Z}_u^{(l)} = \phi(\mathbf{W}_u^{(l)} \mathbf{H}_u^{(l)} + \mathbf{b}_u^{(l)}), \quad \mathbf{Z}_y^{(l)} = \phi(\mathbf{W}_y^{(l)} \mathbf{H}_y^{(l)} + \mathbf{b}_y^{(l)}), \quad l = 1, 2, \dots, L-1 \quad (\text{E.3})$$

$$\mathbf{H}_u^{(l+1)} = (1 - \mathbf{Z}_u^{(l)}) \odot \mathbf{U} + \mathbf{Z}_u^{(l)} \odot \mathbf{V}, \quad l = 1, \dots, L-1 \quad (\text{E.4})$$

$$\mathbf{H}_y^{(l+1)} = (1 - \mathbf{Z}_y^{(l)}) \odot \mathbf{U} + \mathbf{Z}_y^{(l)} \odot \mathbf{V}, \quad l = 1, \dots, L-1 \quad (\text{E.5})$$

$$\mathbf{H}_u^{(L)} = \phi(\mathbf{W}_u^{(L)} \mathbf{H}_u^{(L-1)} + \mathbf{b}_u^{(L)}), \quad \mathbf{H}_y^{(L)} = \phi(\mathbf{W}_y^{(L)} \mathbf{H}_y^{(L-1)} + \mathbf{b}_y^{(L)}) \quad (\text{E.6})$$

$$G_{\theta}(\mathbf{u})(\mathbf{y}) = \langle \mathbf{H}_u^{(L)}, \mathbf{H}_y^{(L)} \rangle, \quad (\text{E.7})$$

where \odot denotes point-wise multiplication, ϕ denotes a activation function, and θ represents all trainable parameters of the DeepONet model. In particular, $\{\mathbf{W}_u^{(l)}, \mathbf{b}_u^{(l+1)}\}_{l=1}^{L+1}$ and $\{\mathbf{W}_y^{(l)}, \mathbf{b}_y^{(l+1)}\}_{l=1}^{L+1}$ are the weights and biases of the branch and trunk networks, respectively. Wang *et al.* [45] have demonstrated that this Modified DeepONet architecture is more resilient against vanishing gradient pathologies and can consistently outperform the conventional architecture put forth by Lu *et al.* [46].

F Validation

We consider Finite Element (FE) solutions in order to validate the DeepONet results to the problem of optimal control of 2D heat equation (section 3.2) and to the problem of drag minimization over an obstacle in Stokes-flow (section 3.3). The FE solutions are generated using the FEniCS solver [52] on a 4-core MacBook Pro laptop (with a 2 GHz Intel CPU and 16 GB RAM).

F.1 Optimal control of 2D heat equation

Since the 2D heat equation is a spatio-temporal PDE, we consider the forward Euler scheme for the finite difference discretization in time, and a finite element (FE) approximation for the space discretization [59, 60].

For the FE approximation, we rely on a continuous Galerkin method. In order to establish the required resolutions for the different discretization parameters, we perform a grid search over: the time step, the FE discretization order, the FE mesh size, and the tolerance of the L-BFGS algorithm. The high-fidelity solution is taken such that the time step is equal to $dt = 0.01$, the mesh size is equal to $h = 0.015625$, the FE discretization is of second order (i.e. \mathbb{P}_2 FE approximation space), and the L-BFGS tolerance is equal to 10^{-12} . The optimal source term u_{HF} obtained with these settings as a solution to the problem (3.8)-(3.12) is considered as the high-fidelity solution, and we perform a grid search over the discretization parameters listed above in order to pick the resolutions that provide an optimal source term u^* with a relative error below 1% compared to u_{HF} . Such criteria provides the following discretization parameters: the time step is equal to $dt = 0.02$, the mesh size is equal to $h = 0.0625$, the FE discretization is of first order (i.e. \mathbb{P}_1 FE approximation space), and the L-BFGS tolerance is equal to 10^{-9} .

Performing the PDE-constrained optimization with the discretization settings obtained with the grid search and specified above (which gives the optimal source term u^*) requires 163 *s* on a 4-core MacBook Pro laptop (with a 2 GHz Intel CPU and 16 GB RAM). The forward pass required to estimate the FE solution with these settings takes 0.37 *s*. As a reference, if one opts for a finer mesh size equal to $h = 0.015625$, as used to obtain the high fidelity solution u_{HF} , then the PDE-constrained optimization takes 605 *s*, while the forward pass takes 2.55 *s*.

F.2 Drag minimization over an obstacle in Stokes-flow

For the FE approximation of the problem of drag minimization over an obstacle in Stokes-flow, the stresses h at the obstacle-fluid boundary $\partial\Gamma$ are taken as the design parameters. In such a setting, the fluid domain changes from its unperturbed state Ω_0 to the new one $\Omega(s) = \{x + s(h) | x \in \Omega_0\}$ where s is the solution to a linear elasticity problem [61, 62]. During the optimization process, the Stokes equation (3.27)-(3.23) is solved by considering the changed fluid domain $\Omega(s)$ and using the stable Taylor-Hood finite element space as test and trial space. We verify that the code recovers the well characterized optimal geometry for the drag minimization over an obstacle in Stokes-flow and which consists of a rugby shaped ball with a 90 degree front and back corners [63].

Performing the PDE-constrained optimization with the FE approximation specified above requires 43.69 *s* on a 4-core MacBook Pro laptop (with a 2 GHz Intel CPU and 16 GB RAM). The forward pass required to estimate the FE solution with these settings takes 0.37 *s*.

G Supplementary Visualizations

G.1 1D Poisson equation

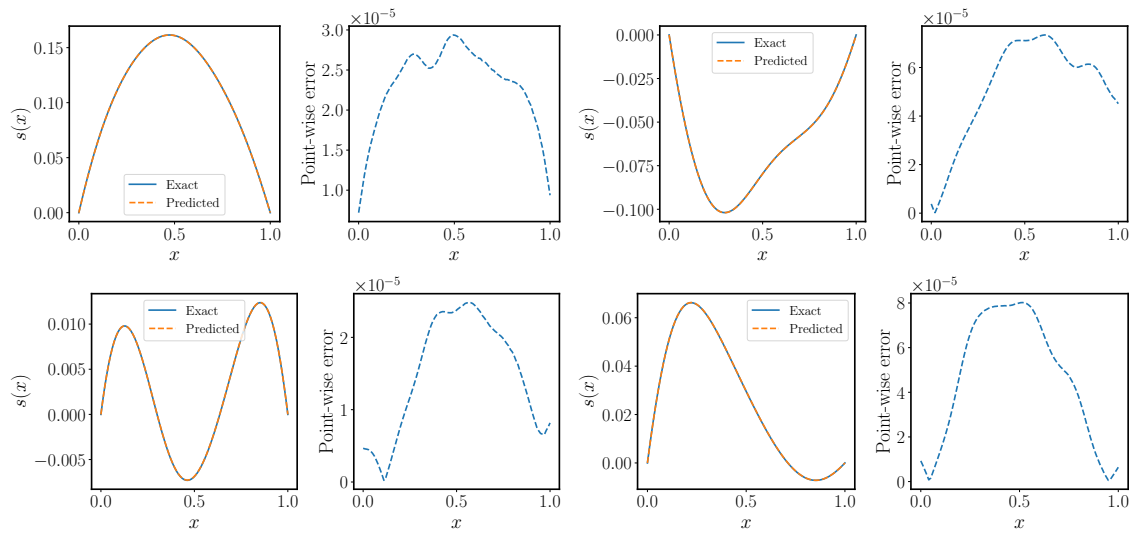


Figure 8: *1D Poisson equation*: Predicted solutions of a trained physics-informed DeepONet for four different examples in the test data-set.

G.2 2D Heat transfer

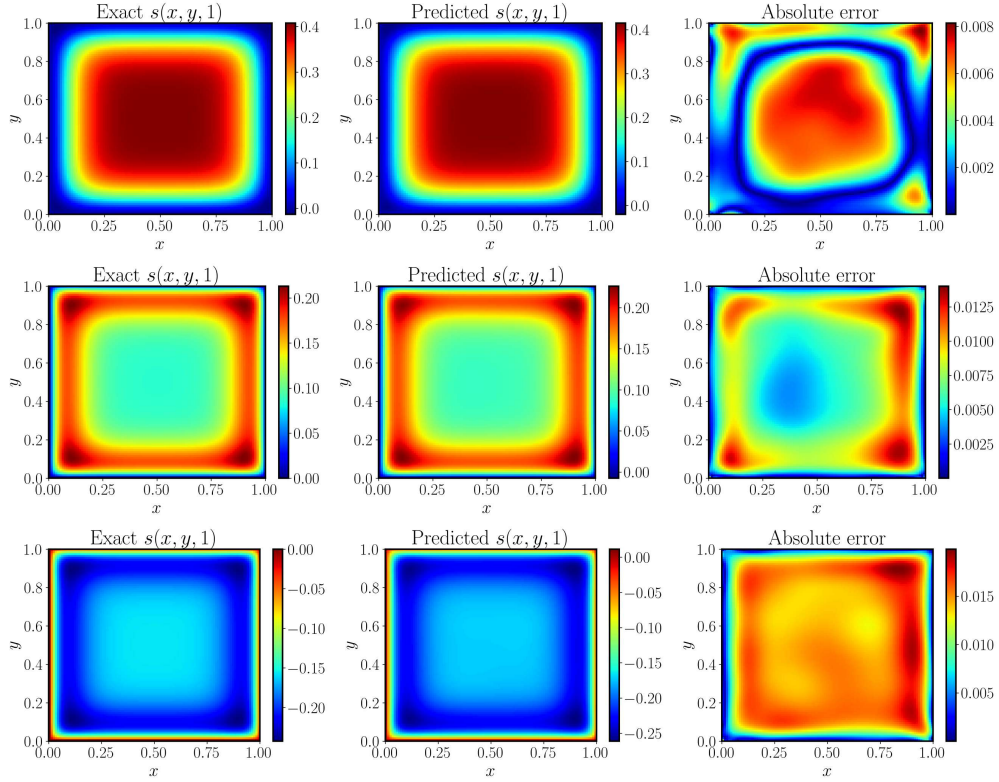
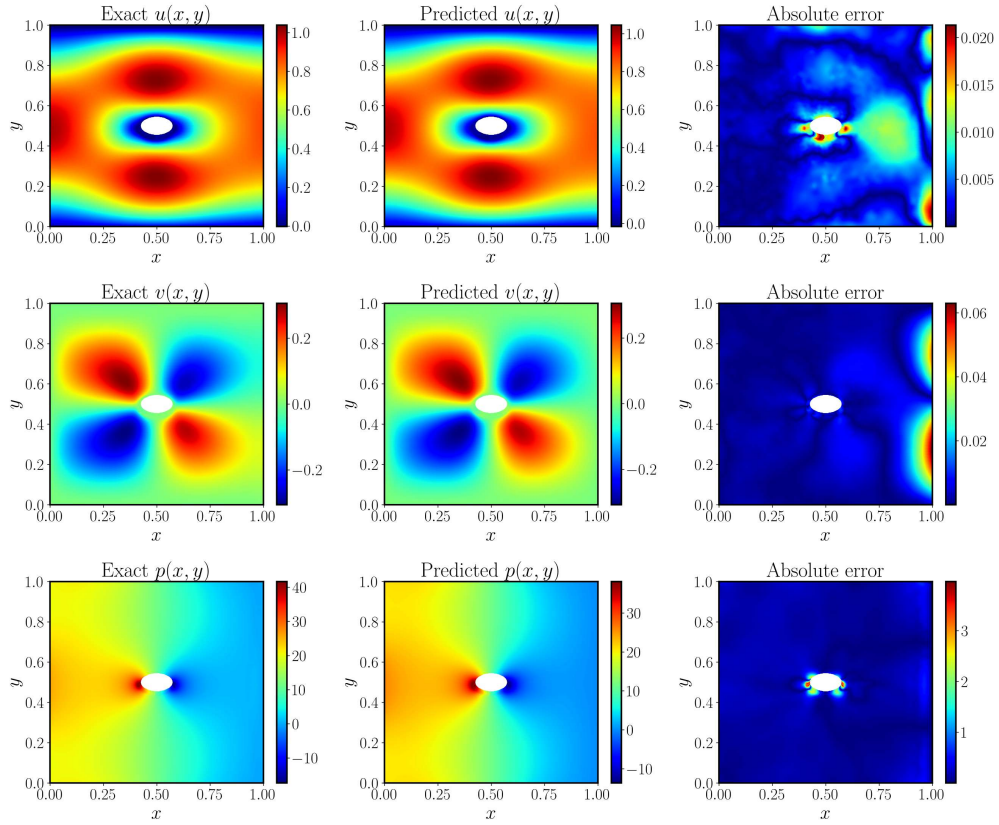


Figure 9: *2D Heat equation*: Comparison of the predicted and exact solutions corresponding to the temporal snapshots at $t = 1$, for three different examples in the test data-set.

G.3 Stokes flow

Figure 10: *Stokes flow*: Predicted solution of a trained physics-informed DeepONet for one example in the test data-set.

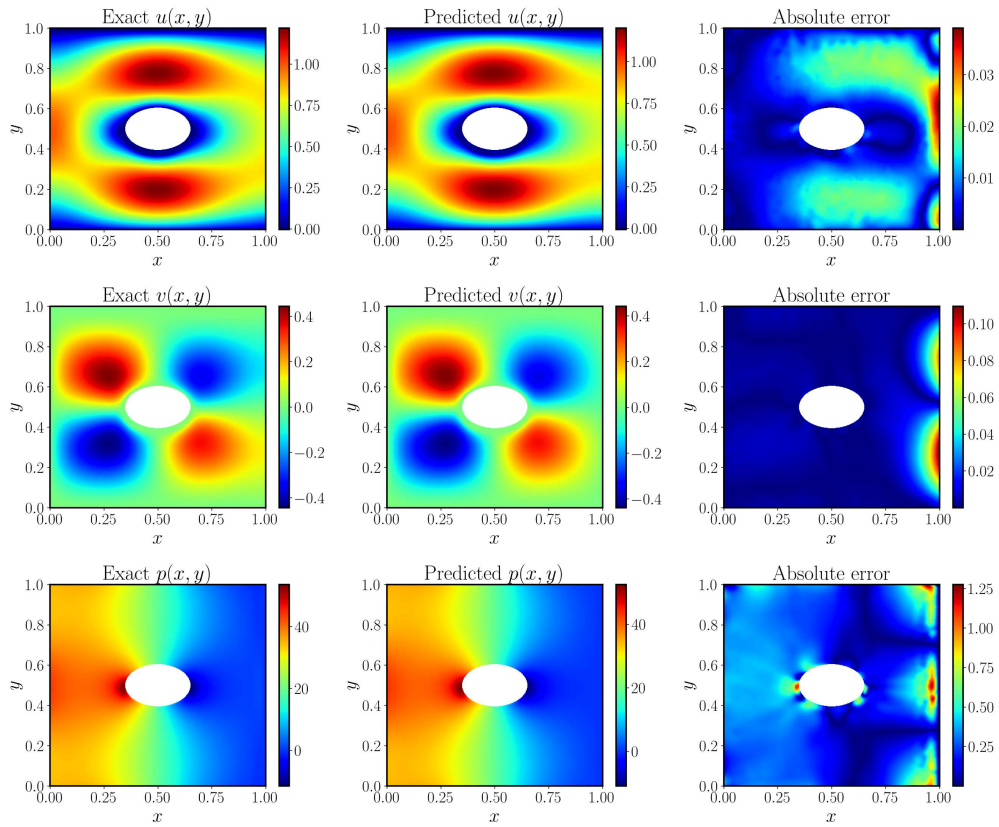


Figure 11: *Stokes flow*: Predicted solution of a trained physics-informed DeepONet for one example in the test data-set.

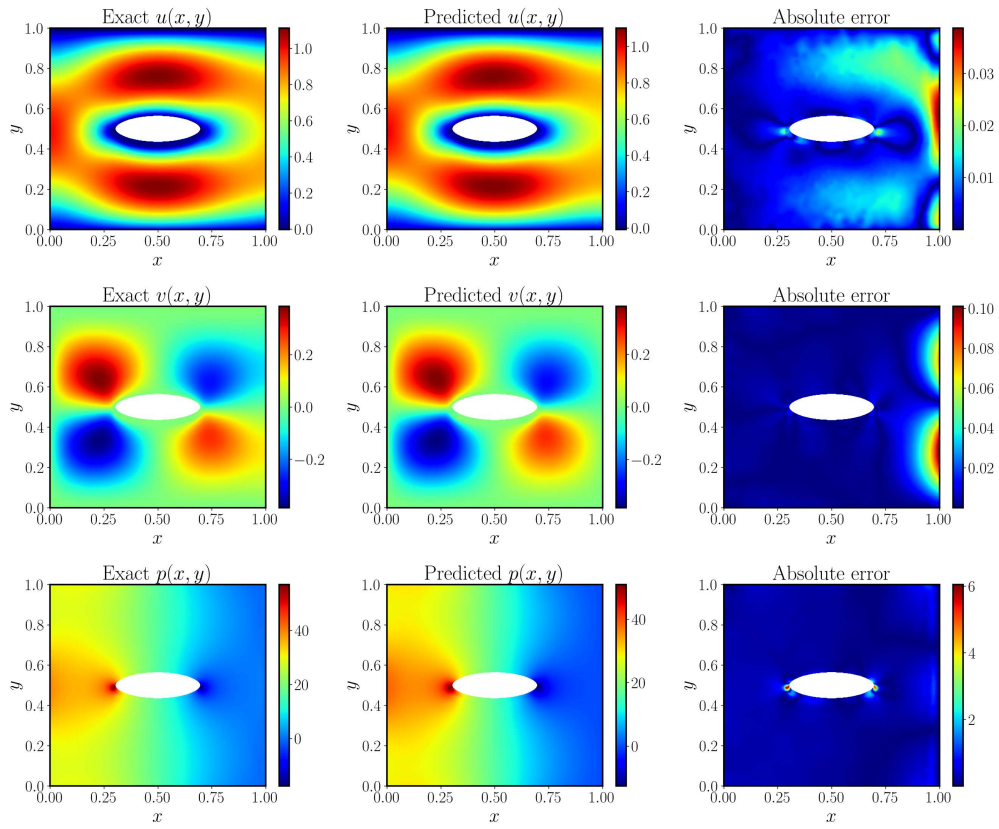


Figure 12: *Stokes flow*: Predicted solution of a trained physics-informed DeepONet for one example in the test data-set.